

Long wave runup on piecewise linear topographies

By UTKU KÂNOĞLU[†] AND
COSTAS EMMANUEL SYNOLAKIS

School of Engineering, University of Southern California, Los Angeles, CA 90089-2531, USA

(Received 29 July 1996 and in revised form 22 December 1997)

We study long-wave evolution and runup on piecewise linear one- and two-dimensional bathymetries analytically and experimentally with the objective of understanding certain coastal effects of tidal waves. We develop a general solution method for determining the amplification factor of different ocean topographies consisting of linearly varying and constant-depth segments to study how spectral distributions evolve over bathymetry, and apply our results to study the evolution of solitary waves. We find asymptotic results which suggest that solitary waves often interact with piecewise linear topographies in a counter-intuitive manner. We compare our analytical predictions with numerical results, with results from a new set of laboratory experiments from a physical model of Revere Beach, and also with the data on wave runup around an idealized conical island. We find good agreement between our theory and the laboratory results for the time histories of free-surface elevations and for the maximum runup heights. Our results suggest that, at least for simple piecewise linear topographies, analytical methods can be used to calculate effectively some important physical parameters in long-wave runup. Also, by underscoring the effects of the topographic slope at the shoreline, this analysis qualitatively suggests why sometimes predictions of field-applicable numerical models differ substantially from observations of tsunami runup.

1. Introduction

Water waves undergo interesting transformations as they evolve over topography and run up on dry beaches. Long water waves generated by impulsive geophysical events – also known as tsunamis or tidal waves – are among the least understood; despite significant advances in understanding their offshore evolution, their runup motions still confound observers and pose non-trivial problems in engineering studies.

For example, in the period 1992–96, eight large nearshore-generated tsunamis caused unexpectedly extensive inundation in the target coastlines. Runup measurements from post-event field surveys suggested that small-scale local bathymetric features affected the runup height to the first order (Satake *et al.* 1993; Yeh *et al.* 1993; Synolakis *et al.* 1995). Interestingly, preliminary modelling predictions undertaken hours after each event and posted on the internet, differed by factors ranging from 2 to 10 from the field data. These large differences could not be attributed to the choice of the friction coefficient which is known to have small effect on runup

[†] Present address: Applied Sciences Laboratory, Inc., 2211 S. Hacienda Blvd., Suite 205, Hacienda Heights, CA 91745, USA.

predictions (Kobayashi & Karjadi 1994; Liu, Synolakis & Yeh 1991), and were probably caused by the absence of detailed runup computations. Until recently (Shuto 1991; Takahashi *et al.* 1995; Liu *et al.* 1995; Titov & Synolakis 1997b), the available field-applicable numerical models stopped calculations at the 10 m depth contour, not only to avoid the notoriously difficult inundation computation, but also because it had seemed reasonable to assume that for long waves of tsunami scales, small changes in bathymetry were unimportant to the first order in their further evolution, beyond that threshold depth.

We set out to investigate these differences, and will present results to demonstrate that certain nearshore bathymetric features are significantly more important than believed earlier. We find that the common engineering practice of routinely estimating the maximum runup of tsunamis by multiplying the offshore wave height at some reference depth by a factor of 2, based on the argument that a long wave interacts with a beach like a shorter wave does with a vertical wall, is inadequate even for qualitative applications. This difficulty along with uncertainties identified recently in the initialization of field-applicable models (Synolakis *et al.* 1997), suggest extreme caution in interpreting modelling results obtained shortly after an event.

We will first briefly discuss several milestones in the calculation of tsunami evolution over topography with one-dimensional and two-dimensional variation, and we will refer to these as the one-plus-one and the two-plus-one evolution problems respectively.

The linear one-plus-one problem of a periodic wave propagating first over constant depth and then up a sloping beach was solved by Keller & Keller (1964). Carrier (1966) presented a general method to calculate long-wave evolution using linear and nonlinear theory and suggested first that the maximum runup predictions are mathematically identical using the linear and nonlinear versions of the shallow water wave equations, but his calculations did not include reflection. Shaw (1974) presented a solution for linear depth variations. Abe & Ishii (1980) and Goring (1978) considered the propagation of tsunamis on a linear slope between two constant-depth segments. Neu & Shaw (1981) examined the transmission and reflection of wave energy by trenches and ridges. Neu & Shaw (1987) examined the filtering action of a submerged seamounts, a trench slope–shelf system and the effect of a continental slope–shelf system alone. Nachbin & Papanicolaou (1992) used a conformal transformation to solve a linearized transmission–reflection channel problem; Carrier’s (1966) and theirs are the only studies which have used waves other than sinusoidal. Synolakis (1987) presented an exact theory for non-breaking waves which offshore had solitary wave profiles, and derived asymptotic results for their maximum runup; he also proved that the runup invariance suggested by Carrier (1966) for periodic waves is also valid for spectral distributions.

The two-plus-one evolution problem has received comparatively less attention. Carrier & Noiseux (1983) calculated the reflection of obliquely incident solitary waves off a plane beach. Carrier (1993) used linear and nonlinear theory to calculate the runup of physically realistic tsunamis on plane beaches. Brocchini & Peregrine (1996) presented a weakly nonlinear and weakly two-plus-one formulation and calculated the runup of tsunamis at small angles of incidence.

Wave runup around islands has received significant attention (Liu *et al.* 1995), since the catastrophe in Babi island (Yeh *et al.* 1993, 1994). Before then, there had been several studies which identified some interesting features of this problem, but never calculated the runup distribution. Longuet-Higgins (1967) suggested that wave

energy trapping depended on the island size and the sea bed topography for long waves. Vastano & Reid (1967) used a numerical integration procedure to evaluate wave amplitude around the perimeter of paraboloidal island, where the depth was proportional to the square of the radial distance up to a prescribed threshold, beyond which it was constant. They compared their numerical results with the laboratory data of Homma (1950) with good agreement. Lautenbacher (1970) analysed the runup problem for a plane and monochromatic wave on a conical island by converting the linear differential equation to an integral equation, which he then solved numerically. Provis (1975) published laboratory data for the runup of sinusoidal waves on a circular island. His results differed substantially from the computations of Smith & Sprinks (1975), who used a mild-slope type equation for incident monochromatic waves. Sprinks & Smith (1983) suggested that the viscous damping and standing waves between the wave generator and the island were responsible for the discrepancies, as in the physical model a 3 m diameter island was placed in a 15 cm deep 5.5 m \times 5.80 m basin. Shaw & Neu (1988) considered axisymmetric topographies where the depth was proportional to r^β for arbitrary β . They found that convex islands with $\beta > 2$ interacted strongly with tsunamis, but that when $\beta < 2$ there was little interaction. They argued that this difference was attributable to the angular velocity of waves which increased with the radius causing the outward spiralling wave to be refracted back inwards toward the centre, as also observed earlier by Longuet-Higgins (1967) and Shen, Meyer & Keller (1968). More recently, Tinti & Vannini (1994) investigated the tsunami propagation around an island, by using n segments, where the depth $h(r)$ was approximated by $H_n(r) = h_j(r/d_j)^{l_j}$ where $h_j = h(d_j)$ and $l_j = \ln(h_j/h_{j+1})/\ln(d_j/d_{j+1})$; their solution involved the inversion of a $2n$ system of equations.

Despite these investigations, no analytical results appropriate for asymptotic analysis exist for long wave amplification even over one-dimensional piecewise linear topography consisting of sloping and constant-depth segments, except in the simplest case of the so-called canonical problem of a sloping beach adjoining a constant-depth segment. This is regrettable, because even though asymptotic results are never as accurate as numerical solutions, they often reveal parameter variations and relevant scaling laws which may not be otherwise evident. Our objective is to derive asymptotic results which will help elucidate how the runup of long waves depends on nearshore topographic features.

We noted that Miles (1967), Devillard, Dunlop & Souillard (1988) and Evans & Linton (1994) used (2×2) transfer-matrix formulations for calculating wave transmission over adjoining regions of constant depth, but they did not address the runup problem at all. Here, we were motivated by the work of Gerrard & Burch (1987) who calculated the propagation of a paraxial ray through an optical system containing n refracting surfaces separated by $(n-1)$ voids. They associated each refracting surface or gap with a rank-2 matrix and they were able to calculate parameters such as the overall amplification factor of the system of lenses only through multiplication of simple (2×2) matrices. Their method is shown in figure 1.

At least for linear theory, the governing equations of water wave evolution are similar to the equations of optics, both being applications of the classic theory of fields. We will therefore present a general method for determining the amplification over fairly arbitrary, piecewise linear topographies, and we will derive asymptotic results for the maximum runup of solitary waves. We will then extend the theory to derive results for wave evolution and runup around a conical island. We will compare our analytical results and our asymptotic predictions with numerical predictions and

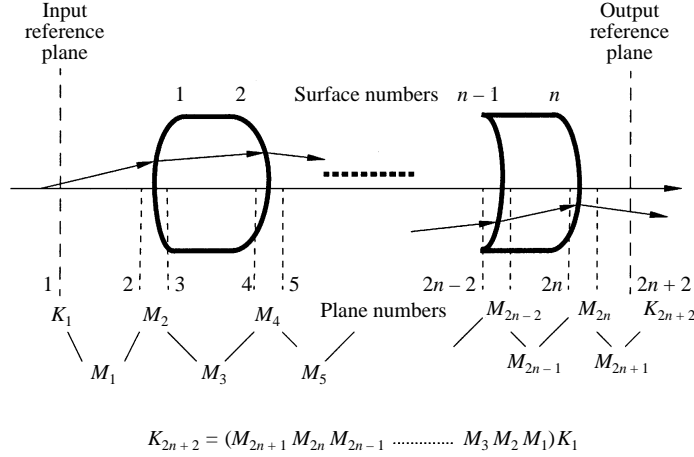


FIGURE 1. Formulation of the propagation of a paraxial ray through an optical system containing n refracting surfaces separated by $(n-1)$ gaps.

with laboratory data from a physical model of Revere Beach in Massachusetts, and from a model of conical island in a large wave basin.

In our analysis, we will use the linear form of the shallow-water wave equations (LSW); their nonlinear form (NSW) has been long believed to be an adequate model for calculating the coastal effects of tsunamis (Liu *et al.* 1991), and at least for the one-dimensional evolution, the runup predictions of linear and nonlinear theory are mathematically identical. We note that Hamilton (1977) has shown that the LSW and the NSW models are not adequate for long-wave propagation over rapidly varying depth; nonetheless, we note that at least for the plane-beach problem, the LSW approximation has been repeatedly shown to produce better than just adequate predictions for pulse evolution, compared with laboratory data (Synolakis 1987). Also, we note that the NSW model is the standard computational model for predicting tsunami coastal effects (Yeh, Liu & Synolakis 1997). We will not present comparisons with numerical results based on the conformal coordinate equation of Hamilton (1977) or with higher-order theories, such as those of Grilli (1996) or Watson, Barnes & Peregrine (1997). Our objective is not to determine whether one particular approximation of the Navier–Stokes equations is superior for predictions than others; instead, our purpose is to derive some simple asymptotic results to help understand which nearshore bathymetric features are physically important. If anything, our results suggest that the runup process is much richer in detail than previously realized, and that detailed inundation computations using higher-order theories are almost invariably necessary for accurate predictions, i.e. the practice of evaluating the coastal effects of tsunamis by models which stop the computations at the 10 m depth contour, or by estimating the upper limit of inundation by multiplying the offshore height by a factor of 2 is inadequate, at least for the cases we will consider here.

2. Basic equations

We use the linear shallow water wave equation that describes a propagation problem in water of variable depth $h_0(x)$ as a field equation. In terms of the free

surface elevation, $\eta = \eta(x, t)$, the field equation is

$$\eta_{tt} - (\eta_x h_0)_x = 0. \quad (2.1)$$

Here we used the undisturbed water depth d over which the incident wave field travels initially to introduce dimensionless variables; i.e. $x = \tilde{x}/d$, $h = \tilde{h}/d$, $\eta = \tilde{\eta}/d$, $u = \tilde{u}/(gd)^{1/2}$, $t = \tilde{t}/(gd)^{1/2}$, $\omega = \tilde{\omega}/(gd)^{1/2}$.

2.1. Formulation of the solution

We assume a time-harmonic dependence of the form, $\mathcal{A}(x)e^{-i\omega t}$. Then, the linear field equation becomes

$$h_0(x) \frac{d^2 \mathcal{A}(x)}{dx^2} + \frac{dh_0(x)}{dx} \frac{d\mathcal{A}(x)}{dx} + \omega^2 \mathcal{A}(x) = 0, \quad (2.2)$$

which has different eigenfunctions for different topographies $h_0(x)$. The eigenfunctions of the field equation for wave propagation over a segment of constant depth $h_0(x) = h_c$ are

$$\eta(x, t) = \left\{ A^{(1)} \exp\left(-\frac{i\omega x}{h_c^{1/2}}\right) + B^{(1)} \exp\left(\frac{i\omega x}{h_c^{1/2}}\right) \right\} e^{-i\omega t}, \quad (2.3)$$

where $A^{(1)}$ and $B^{(1)}$ are arbitrary constants. In segments of linearly varying depth $h_0(x) = mx + n$, where $m \neq 0$ and n are constant, the eigenfunctions of the field equation are $\mathfrak{I}_0(2\omega\xi^{1/2})$ which are two zeroth-order linearly-independent solutions of Bessel's equation and $\xi = (x + n/m)/m$. Therefore, the solution for segments of linearly varying depth is

$$\eta(x, t) = \{A^{(2)}J_0(2\omega\xi^{1/2}) + B^{(2)}Y_0(2\omega\xi^{1/2})\} e^{-i\omega t}, \quad (2.4)$$

where $A^{(2)}$ and $B^{(2)}$ are arbitrary constants. We note that this solution is valid whether the segment is sloping positively or negatively with respect to the datum.

A standard solution would consist of representing a given piecewise linear topography by a series of constant-depth or linearly-varying-depth segments extending from the seaward boundary to the initial shoreline. From the basic solutions (2.3) and (2.4), the appropriate form of η would be chosen for each segment. The two boundary conditions of continuity of the surface amplitude and its x -slope between adjacent segments at the interface provide two equations for the coefficients of equations (2.3) and (2.4), which of course are *a priori* unknown. In general a topography with m segments would require the solution of $(2m - 1)$ equations for the $(2m - 1)$ coefficients in the sets of equations like (2.3) and (2.4). One problem with the formulation above is that it does not allow explicit analytic determination of any of the unknown coefficients, except for the simplest one-segment topography. In practice, the coefficients of interest are only the overall transmission coefficient and the overall reflection coefficient, yet the standard method would require the inversion of the $(2m - 1) \times (2m - 1)$ matrix. Since this is done numerically, the derivation of asymptotic results is impractical.

Motivated by the analogy with geometric optics, we will develop a simpler method to allow explicit determination of the parameters of interest. One example of this process is presented in the next section for a continental slope and shelf topogra-

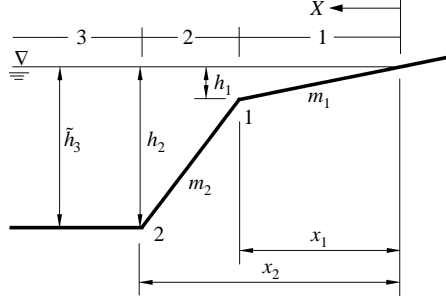


FIGURE 2. Definition sketch for the continental shelf and slope topography.

phy; after this example, we will develop a general methodology for piecewise linear bathymetries, and then we will present a series of laboratory data to assess the accuracy of our method.

2.2. Continental slope and shelf

We consider a continental slope and shelf topography similar to that studied by Neu & Shaw (1987) for sinusoidal waves. The topography is shown in figure 2 and it consists of three segments, which are a linearly sloping continental shelf extending from $x = 0$ to $x = x_1$, a continental slope segment extending from $x = x_1$ to $x = x_2$ and a constant-depth segment where the incident wave which has the amplitude A_i travels. Choosing the characteristic normalization length as the dimensional depth of the constant-depth segment \tilde{h}_3 , we match the solutions in the two transition points x_1 and x_2 , and derive the following matching conditions, i.e. continuity of the free surface elevation and of the slope:

(i) at $x = x_1$, boundary conditions require

$$A^{(1)} J_0 \left(\frac{2\omega h_1^{1/2}}{m_1} \right) = A^{(2)} J_0 \left(\frac{2\omega h_1^{1/2}}{m_2} \right) + B^{(2)} Y_0 \left(\frac{2\omega h_1^{1/2}}{m_2} \right), \quad (2.5)$$

$$A^{(1)} J_1 \left(\frac{2\omega h_1^{1/2}}{m_1} \right) = A^{(2)} J_1 \left(\frac{2\omega h_1^{1/2}}{m_2} \right) + B^{(2)} Y_1 \left(\frac{2\omega h_1^{1/2}}{m_2} \right); \quad (2.6)$$

(ii) at $x = x_2$, the boundary conditions require

$$A^{(2)} J_0 \left(\frac{2\omega h_2^{1/2}}{m_2} \right) + B^{(2)} Y_0 \left(\frac{2\omega h_2^{1/2}}{m_2} \right) = A_i \exp \left(-\frac{i\omega x_2}{h_3^{1/2}} \right) + A_r \exp \left(\frac{i\omega x_2}{h_3^{1/2}} \right), \quad (2.7)$$

$$A^{(2)} J_1 \left(\frac{2\omega h_2^{1/2}}{m_2} \right) + B^{(2)} Y_1 \left(\frac{2\omega h_2^{1/2}}{m_2} \right) = A_i i \exp \left(-\frac{i\omega x_2}{h_3^{1/2}} \right) - A_r i \exp \left(\frac{i\omega x_2}{h_3^{1/2}} \right). \quad (2.8)$$

Notice that in the first segment the requirement of the boundedness of the solution at the shoreline implies a zero coefficient $B^{(1)}$ for the Bessel function. The coefficients

$A^{(1)}$, $A^{(2)}$, $B^{(2)}$ and A_r are evaluated by solving the system

$$\begin{pmatrix} -J_0\left(\frac{2\omega h_1^{1/2}}{m_1}\right) & J_0\left(\frac{2\omega h_1^{1/2}}{m_2}\right) & Y_0\left(\frac{2\omega h_1^{1/2}}{m_2}\right) & 0 \\ -J_1\left(\frac{2\omega h_1^{1/2}}{m_1}\right) & J_1\left(\frac{2\omega h_1^{1/2}}{m_2}\right) & Y_1\left(\frac{2\omega h_1^{1/2}}{m_2}\right) & 0 \\ 0 & J_0\left(\frac{2\omega h_2^{1/2}}{m_2}\right) & Y_0\left(\frac{2\omega h_2^{1/2}}{m_2}\right) & -\exp\left(\frac{i\omega x_2}{h_3^{1/2}}\right) \\ 0 & J_1\left(\frac{2\omega h_2^{1/2}}{m_2}\right) & Y_1\left(\frac{2\omega h_2^{1/2}}{m_2}\right) & i \exp\left(\frac{i\omega x_2}{h_3^{1/2}}\right) \end{pmatrix} \begin{pmatrix} A^{(1)} \\ A^{(2)} \\ B^{(2)} \\ A_r \end{pmatrix} = \begin{pmatrix} 0 \\ 0 \\ \exp\left(-\frac{i\omega x_2}{h_3^{1/2}}\right) \\ i \exp\left(-\frac{i\omega x_2}{h_3^{1/2}}\right) \end{pmatrix} A_i. \quad (2.9)$$

Note that in practice only the reflection coefficient A_r and $A^{(1)}$ are of interest; once $A^{(1)}$ is known the runup can be determined, and because of its importance we will henceforth denote $A^{(1)}$ by \mathcal{B} . Even in this simplest case of a two-segment topography, the system (2.9) does not allow for closed-form solutions.

Alternatively, note that in matrix form, the matching conditions (2.5) and (2.6) can be rewritten as

$$\begin{pmatrix} J_0\left(\frac{2\omega h_1^{1/2}}{m_1}\right) \\ J_1\left(\frac{2\omega h_1^{1/2}}{m_1}\right) \end{pmatrix} \mathcal{B} = \begin{pmatrix} J_0\left(\frac{2\omega h_1^{1/2}}{m_2}\right) & Y_0\left(\frac{2\omega h_1^{1/2}}{m_2}\right) \\ J_1\left(\frac{2\omega h_1^{1/2}}{m_2}\right) & Y_1\left(\frac{2\omega h_1^{1/2}}{m_2}\right) \end{pmatrix} \begin{pmatrix} A^{(2)} \\ B^{(2)} \end{pmatrix}, \quad (2.10)$$

and denoting the column vector on the left as S_{11} , the unknown scalar on the left as V_1 , the matrix on the right as S_{12} and the unknown vector on the right as V_2 the following matrix equation can be written:

$$S_{11}V_1 = S_{12}V_2. \quad (2.11)$$

Here it is important to note that the boundedness of the solution at the coastline forces S_{11} to be a column vector and V_1 to be the scalar amplification factor \mathcal{B} . From the boundary conditions (2.7) and (2.8), the following matrix equations can be

written:

$$\begin{aligned} \begin{pmatrix} J_0 \left(\frac{2\omega h_2^{1/2}}{m_2} \right) & Y_0 \left(\frac{2\omega h_2^{1/2}}{m_2} \right) \\ J_1 \left(\frac{2\omega h_2^{1/2}}{m_2} \right) & Y_1 \left(\frac{2\omega h_2^{1/2}}{m_2} \right) \end{pmatrix} \begin{pmatrix} A^{(2)} \\ B^{(2)} \end{pmatrix} \\ = \begin{pmatrix} \exp \left(-\frac{i\omega x_2}{h_3^{1/2}} \right) & \exp \left(\frac{i\omega x_2}{h_3^{1/2}} \right) \\ i \exp \left(-\frac{i\omega x_2}{h_3^{1/2}} \right) & -i \exp \left(\frac{i\omega x_2}{h_3^{1/2}} \right) \end{pmatrix} \begin{pmatrix} A_i \\ A_r \end{pmatrix}, \end{aligned} \quad (2.12)$$

and again, from left to right denoting the matrices S_{22} and D_{23} and the unknown column vectors V_2 and V_3 respectively, one obtains

$$S_{22}V_2 = D_{23}V_3. \quad (2.13)$$

Combining the two matrix equations (2.10) and (2.12), the amplification factor \mathcal{B} and the reflection coefficient A_r can be found in terms of the initial wave amplitude A_i by,

$$\begin{aligned} \begin{pmatrix} J_0 \left(\frac{2\omega h_1^{1/2}}{m_1} \right) \\ J_1 \left(\frac{2\omega h_1^{1/2}}{m_1} \right) \end{pmatrix} \mathcal{B} = \begin{pmatrix} J_0 \left(\frac{2\omega h_1^{1/2}}{m_2} \right) & Y_0 \left(\frac{2\omega h_1^{1/2}}{m_2} \right) \\ J_1 \left(\frac{2\omega h_1^{1/2}}{m_2} \right) & Y_1 \left(\frac{2\omega h_1^{1/2}}{m_2} \right) \end{pmatrix} \begin{pmatrix} J_0 \left(\frac{2\omega h_2^{1/2}}{m_2} \right) & Y_0 \left(\frac{2\omega h_2^{1/2}}{m_2} \right) \\ J_1 \left(\frac{2\omega h_2^{1/2}}{m_2} \right) & Y_1 \left(\frac{2\omega h_2^{1/2}}{m_2} \right) \end{pmatrix}^{-1} \\ \times \begin{pmatrix} \exp \left(-\frac{i\omega x_2}{h_3^{1/2}} \right) & \exp \left(\frac{i\omega x_2}{h_3^{1/2}} \right) \\ i \exp \left(-\frac{i\omega x_2}{h_3^{1/2}} \right) & -i \exp \left(\frac{i\omega x_2}{h_3^{1/2}} \right) \end{pmatrix} \begin{pmatrix} A_i \\ A_r \end{pmatrix}. \end{aligned} \quad (2.14)$$

Using again the matrix notation introduced, we write

$$S_{11}\mathcal{B} = S_{12}S_{22}^{-1}D_{23}V_3, \quad (2.15)$$

a matrix equation which allows direct evaluation of the amplification factor \mathcal{B} and the reflection coefficient A_r in terms of the initial wave amplitude A_i , explicitly by multiplication of simple (2×2) matrices.

As an example of the calculation of the evolution of spectral distributions, consider a solitary wave profile propagating initially over constant depth and approaching the composite beach. A solitary wave located at $x = x_s$ at $t = 0$ has a surface profile given by $\eta(x, 0) = H \operatorname{sech}^2 \gamma(x - x_s)$, where H is the solitary wave height and $\gamma = (3H/4)^{1/2}$. $\Phi(\omega)$ – the Fourier transform of the initial surface profile – associated with this $\eta(x, 0)$ is given by $\Phi(\omega) = (2/3)\omega \operatorname{cosech}(\alpha\omega) e^{i\omega x_s}$, with $\alpha = \pi/2\gamma$, Synolakis (1987). Then the transmitted wave to the beach is given by

$$\eta_1(x, t) = \int_{-\infty}^{+\infty} \Phi(\omega) \mathcal{B}(\omega) J_0 \left(\frac{2\omega(h_1(x))^{1/2}}{m_1} \right) e^{-i\omega t} d\omega. \quad (2.16)$$

In the case of the topography of figure 2, the amplification factor $\mathcal{B}(\omega)$ is found through the Wronskian identity as

$$\mathcal{B} = -\frac{2m_2}{\pi\omega h_1^{1/2}} \frac{1}{\varphi_c + i\chi_c} \exp\left(-\frac{i\omega x_2}{h_3^{1/2}}\right), \quad (2.17)$$

where

$$\begin{aligned} \varphi_c(\omega) + i\chi_c(\omega) = & \begin{vmatrix} J_0\left(\frac{2\omega h_1^{1/2}}{m_1}\right) & Y_0\left(\frac{2\omega h_1^{1/2}}{m_2}\right) \\ J_1\left(\frac{2\omega h_1^{1/2}}{m_1}\right) & Y_1\left(\frac{2\omega h_1^{1/2}}{m_2}\right) \end{vmatrix} \left\{ J_0\left(\frac{2\omega h_2^{1/2}}{m_2}\right) - iJ_1\left(\frac{2\omega h_2^{1/2}}{m_2}\right) \right\} \\ & - \begin{vmatrix} J_0\left(\frac{2\omega h_1^{1/2}}{m_1}\right) & J_0\left(\frac{2\omega h_1^{1/2}}{m_2}\right) \\ J_1\left(\frac{2\omega h_1^{1/2}}{m_1}\right) & J_1\left(\frac{2\omega h_1^{1/2}}{m_2}\right) \end{vmatrix} \left\{ Y_0\left(\frac{2\omega h_2^{1/2}}{m_2}\right) - iY_1\left(\frac{2\omega h_2^{1/2}}{m_2}\right) \right\}. \end{aligned} \quad (2.18)$$

Using the procedure described in Synolakis (1986, 1987), we find that the amplitude at the initial shoreline is given by

$$\mathcal{R}(t) = \eta(0, t) = -\frac{(4/3)m_2}{\pi h_1^{1/2}} \int_{-\infty}^{+\infty} \operatorname{cosech}(\alpha\omega) \frac{1}{\varphi_c + i\chi_c} e^{i\omega(x_s - x_2 - t)} d\omega; \quad (2.19)$$

the maximum value of this integral is the maximum runoff \mathcal{R} . We proceed to evaluate the integral analytically to attempt the determination of the explicit dependence of \mathcal{R} on the problem parameters, i.e. H , m_1 , m_2 , h_1 , h_2 . Here, $\varphi_c(\omega)$ and $\chi_c(\omega)$ are rather complicated expressions of Bessel functions of the first and second kind; we conjecture that $\varphi_c(\omega) + i\chi_c(\omega)$ is an entire function in the upper half-plane, and therefore the poles of the integrand are the poles of $\operatorname{cosech}(\alpha\omega)$. The residue a_n at the poles, $\omega_n = n\pi i/\alpha$, is given by

$$a_n = (-1)^n \left(\frac{1}{\alpha}\right) \frac{e^{-(n\pi/\alpha)(x_s - x_2 - t)}}{\varphi_c(n\pi i/\alpha) + i\chi_c(n\pi i/\alpha)}. \quad (2.20)$$

By the Cauchy integral formula,

$$\mathcal{R}(t) = -\frac{(8/3)m_2}{h_1^{1/2}} i \sum_{n=1}^{+\infty} (-1)^n \left(\frac{1}{\alpha}\right) \frac{e^{-(n\pi/\alpha)(x_s - x_2 - t)}}{\varphi_c(n\pi i/\alpha) + i\chi_c(n\pi i/\alpha)}. \quad (2.21)$$

Since $(n\pi/\alpha)/m_i \gg 1$, for either $i = 1, 2$, we use the asymptotic expansion of the Bessel functions for large arguments, i.e. $J_\nu(z) \sim (2/\pi z)^{1/2}$ and $Y_\nu(z) \sim (2/\pi z)^{1/2}$, in (2.18), and we find that $\varphi_c + i\chi_c \sim m_2 m_1^{1/2}/h_1^{1/2}$; then

$$\begin{aligned} \mathcal{R}(t) = & \frac{8(\pi\sqrt{3})^{1/2}}{m_1^{1/2}} H^{5/4} \sum_{n=1}^{+\infty} (-1)^{n+1} n^{3/2} \\ & \times \exp\left(-\frac{n\pi}{\alpha} \left(x_s - x_2 - t + 2 \left\{ \frac{h_1^{1/2}}{m_1} + \frac{h_2^{1/2} - h_1^{1/2}}{m_2} \right\}\right)\right). \end{aligned} \quad (2.22)$$

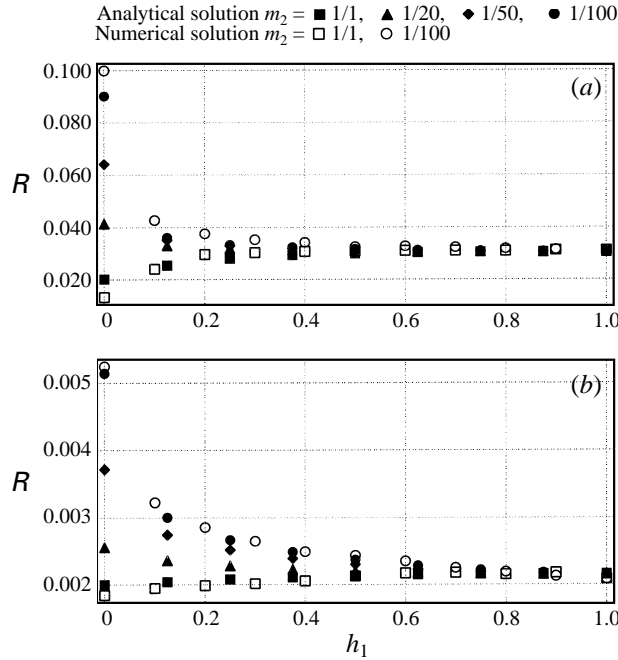


FIGURE 3. The effect of the parameters m_2 , h_1 and H on the maximum runup for the continental shelf and slope with $m_1 = 1/10$. (a) $H = 0.01$, (b) $H = 0.001$.

The maximum of this series of the form $\sum (-1)^{n+1} n^{3/2} \mathcal{G}^n$ is equal to 0.152. Then, the maximum runup is given by

$$R = 2.831 H^{5/4} / m_1^{1/2}. \quad (2.23)$$

Note that this is the same analytical expression that Synolakis (1987) found for the single-slope case, implying that only the slope of the segment closest to the shoreline affects the runup. However, in contrast to Synolakis' (1987) analysis where the asymptotic expansion of $J_0(n\pi i/\alpha) - iJ_1(n\pi i/\alpha)$ was used, the asymptotic expansion of $\varphi_c(n\pi i/\alpha) + i\chi_c(n\pi i/\alpha)$ also involves the depth at the transition point h_1 and two different slopes m_1 and m_2 . Given this counter-intuitive nature of the asymptotic result (2.23), we will compare its predictions both with numerical evaluations of the runup integral (2.19) and with numerical solutions of the NSW equations.

Figure 3 shows the maximum runup results as a function of the depth at the transition point for two different wave heights and for four different topographies, i.e. a 1:10 beach slope closest to the shoreline, fronted by 1:1, or 1:20, or 1:50, or 1:100 slopes. In all cases, when the dimensional depth at the transition point between the two slopes \tilde{h}_1 is greater than half the dimensional depth \tilde{h}_3 of the constant-depth segment, then the runup of the solitary waves appears to be affected only by the slope closest to the shoreline, as suggested by the asymptotic result (2.23). As \tilde{h}_1 decreases, i.e. the length of the slope closest to the shoreline decreases, the effect of m_2 starts to be felt; when $\tilde{h}_1 = 0$, there is no longer any m_1 slope, and the runup result predicted for a single plane beach is recovered. Notice also that this effect is more pronounced for the $H = 0.001$ wave which is longer than the $H = 0.01$ wave. For the $H = 0.01$ wave, the effect of the second slope m_2 is not realized until $h_1 = 0.3$; for $H = 0.001$, the effect of m_2 becomes significant at $h_1 = 0.5$. Clearly neither of the two waves

interacts with this topography as it would with a vertical wall, as might have been anticipated based on simplistic expectations of the behaviour of long waves.

To further validate our observations and to ensure that it was not an artifact of the linear theory or of the asymptotic analysis, we performed numerical experiments using the solution method of the NSW equations referred to as VTCS-2 (Titov & Synolakis 1995; Titov 1997). This method included inundation computations and it has been shown in excellent agreement with laboratory data for solitary waves in this range of parameters. Figure 3 shows the predictions of VTCS-2 for two of the slope combinations. Whereas there are small differences between the VTCS-2 NSW predictions and our LSW results, the overall agreement is satisfactory and provides confidence in using this LSW matrix formulation, again in this parameter range.

3. General method of solution

The analysis of the previous section suggests a general methodology for solving evolution problems over piecewise linear bathymetry. We note that most topographies can be described adequately in terms of three linear basic topographic segments: a constant-depth segment, a positively-sloping segment and a negatively-sloping segment. With each constant-depth segment of depth h_r , we associate a segment matrix D_{pr} given by

$$D_{pr} = \begin{pmatrix} \exp\left(-\frac{i\omega x_p}{h_r^{1/2}}\right) & \exp\left(\frac{i\omega x_p}{h_r^{1/2}}\right) \\ i \exp\left(-\frac{i\omega x_p}{h_r^{1/2}}\right) & -i \exp\left(\frac{i\omega x_p}{h_r^{1/2}}\right) \end{pmatrix}, \quad (3.1)$$

while for each linearly-varying-depth segment with positive slope m_r , we associate a segment matrix S_{pr} given by

$$S_{pr} = \begin{pmatrix} J_0\left(\frac{2\omega h_p^{1/2}}{m_r}\right) & Y_0\left(\frac{2\omega h_p^{1/2}}{m_r}\right) \\ J_1\left(\frac{2\omega h_p^{1/2}}{m_r}\right) & Y_1\left(\frac{2\omega h_p^{1/2}}{m_r}\right) \end{pmatrix}, \quad (3.2)$$

and for each linearly-varying-depth segment with negative slope m_r , we associate a segment matrix S_{pr} given by

$$S_{pr} = \begin{pmatrix} J_0\left(\frac{2\omega h_p^{1/2}}{|m_r|}\right) & Y_0\left(\frac{2\omega h_p^{1/2}}{|m_r|}\right) \\ -J_1\left(\frac{2\omega h_p^{1/2}}{|m_r|}\right) & -Y_1\left(\frac{2\omega h_p^{1/2}}{|m_r|}\right) \end{pmatrix}. \quad (3.3)$$

In all three types of segment matrices, the first subscript p identifies the transition point, and the second subscript r identifies the segment; the indices are incremented arithmetically seawards from the shoreline.

Let the piecewise linear topography consist of m segments, and let Q_{pr} identify the (2×2) matrix of the r th segment at the p th transition point. The segment matrix closest to the shoreline is Q_{11} , and the last segment matrix at the seaward boundary is $Q_{(m-1)m}$. Let $V_m = (A_i, A_r)$, a column vector with elements the incident wave height

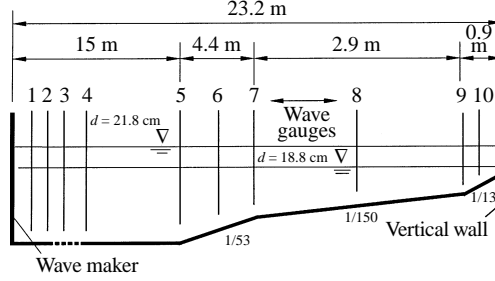


FIGURE 4. A sketch of the Revere Beach topography. This drawing is not to scale.

A_i and the reflected wave height A_r . Let $V_1 = (\mathcal{B}, 0)$ be the column vector closest to the shoreline, where \mathcal{B} is the amplification factor in the first segment. After some algebra, it is possible to show that

$$Q_{11} V_1 = \left\{ \prod_{j=1}^{m-2} Q_{j(j+1)} Q_{(j+1)(j+1)}^{-1} \right\} Q_{(m-1)m} V_m. \quad (3.4)$$

Here Q_{pr} can be either of form D_{pr} or S_{pr} . Notice that equation (3.4) is equivalent to the system of equations which must be solved in the classical method of solution. Moreover, it allows an explicit analytic determination of the two unknowns, the reflected wave amplitude A_r of vector V_m and the amplification factor \mathcal{B} of vector V_1 , because it only involves the inversion of an algebraic product of (2×2) matrices.

A more general form of equation (3.4) can also be written, if one considers a discontinuity of the depth Δh_j at a connection point, corresponding to a vertical step-like feature. In this case, the second row of the segment matrices Q_{jj} must be multiplied by $h_j^{1/2}$ and the second row of $Q_{j(j+1)}$ by $(h_j + \Delta h_j)^{1/2}$.

4. Applications of the theory

4.1. One-dimensional topography, the Revere Beach

The Revere Beach is located approximately six miles northeast of Boston in the City of Revere, Massachusetts. To address beach erosion and severe flooding problems, a physical model of the beach was constructed at the US Army Corps of Engineers, Coastal Engineering Research Center facility in Vicksburg, Mississippi, in a 23.2 m long by 45 cm wide glass, walled flume by Ward (1995). The model consists of three different slopes, 1:53, 1:150 and 1:13 from seaward to shoreward respectively. Figure 4 is a sketch of the physical model which presented a unique opportunity to evaluate the predictions of the general method presented in §3.

4.1.1. Analytical solution

The model of Revere Beach consists of four topographic segments ($m = 4$) starting from the wall at the shoreline, and therefore equation (3.4) becomes

$$S_{11} V_1 = S_{12} S_{22}^{-1} S_{23} S_{33}^{-1} D_{34} V_4, \quad (4.1)$$

where $V_1 = (A^{(1)}, B^{(1)})$ and $V_4 = (A_i, A_r)$. Note that this is a slightly more difficult case, because the vertical wall at the shoreline requires non-zero coefficients for both eigenfunctions at the segment closest to the shoreline. The condition of perfect

reflection at the vertical wall allows us to write the following matrix equation:

$$V_1 = S_1 A^{(1)}, \quad (4.2)$$

with expanded form

$$\begin{pmatrix} A^{(1)} \\ B^{(1)} \end{pmatrix} = \begin{pmatrix} 1 \\ -J_1 \left(\frac{2\omega h_w^{1/2}}{m_1} \right) / Y_1 \left(\frac{2\omega h_w^{1/2}}{m_1} \right) \end{pmatrix} A^{(1)}. \quad (4.3)$$

Therefore, equation (4.1) takes the form

$$S_1 A^{(1)} = S_{11}^{-1} S_{12} S_{22}^{-1} S_{23} S_{33}^{-1} D_{34} V_4. \quad (4.4)$$

In expanded form, this equation is

$$\begin{aligned} & \begin{pmatrix} 1 \\ -J_1 \left(\frac{2\omega h_w^{1/2}}{m_1} \right) / Y_1 \left(\frac{2\omega h_w^{1/2}}{m_1} \right) \end{pmatrix} A^{(1)} \\ &= \begin{pmatrix} J_0 \left(\frac{2\omega h_1^{1/2}}{m_1} \right) & Y_0 \left(\frac{2\omega h_1^{1/2}}{m_1} \right) \\ J_1 \left(\frac{2\omega h_1^{1/2}}{m_1} \right) & Y_1 \left(\frac{2\omega h_1^{1/2}}{m_1} \right) \end{pmatrix}^{-1} \begin{pmatrix} J_0 \left(\frac{2\omega h_1^{1/2}}{m_2} \right) & Y_0 \left(\frac{2\omega h_1^{1/2}}{m_2} \right) \\ J_1 \left(\frac{2\omega h_1^{1/2}}{m_2} \right) & Y_1 \left(\frac{2\omega h_1^{1/2}}{m_2} \right) \end{pmatrix} \\ &\times \begin{pmatrix} J_0 \left(\frac{2\omega h_2^{1/2}}{m_2} \right) & Y_0 \left(\frac{2\omega h_2^{1/2}}{m_2} \right) \\ J_1 \left(\frac{2\omega h_2^{1/2}}{m_2} \right) & Y_1 \left(\frac{2\omega h_2^{1/2}}{m_2} \right) \end{pmatrix}^{-1} \begin{pmatrix} J_0 \left(\frac{2\omega h_2^{1/2}}{m_3} \right) & Y_0 \left(\frac{2\omega h_2^{1/2}}{m_3} \right) \\ J_1 \left(\frac{2\omega h_2^{1/2}}{m_3} \right) & Y_1 \left(\frac{2\omega h_2^{1/2}}{m_3} \right) \end{pmatrix} \\ &\times \begin{pmatrix} J_0 \left(\frac{2\omega h_3^{1/2}}{m_3} \right) & Y_0 \left(\frac{2\omega h_3^{1/2}}{m_3} \right) \\ J_1 \left(\frac{2\omega h_3^{1/2}}{m_3} \right) & Y_1 \left(\frac{2\omega h_3^{1/2}}{m_3} \right) \end{pmatrix}^{-1} \begin{pmatrix} \exp \left(-\frac{i\omega x_3}{h_4^{1/2}} \right) & \exp \left(\frac{i\omega x_3}{h_4^{1/2}} \right) \\ i \exp \left(-\frac{i\omega x_3}{h_4^{1/2}} \right) & -i \exp \left(\frac{i\omega x_3}{h_4^{1/2}} \right) \end{pmatrix} \begin{pmatrix} A_i \\ A_r \end{pmatrix}. \end{aligned} \quad (4.5)$$

Consider a long wave with a solitary wave profile at the constant-depth segment; as before, the wave elevation at the shoreline is given by

$$\mathcal{R}(t) = \eta(0, t) = -\frac{(4/3)m_1}{\pi h_w^{1/2}} \int_{-\infty}^{+\infty} \operatorname{cosech}(\alpha\omega) \frac{1}{\varphi_r + i\chi_r} e^{i\omega(x_s - x_3 - t)} d\omega. \quad (4.6)$$

Again, to determine the parametric dependence of \mathcal{R} on parameters of the problem integral (4.6) must be evaluated analytically. As before, by the Cauchy integral formula,

$$\mathcal{R}(t) = -\frac{(8/3)m_1}{h_w^{1/2}} i \sum_{n=1}^{+\infty} (-1)^n \left(\frac{1}{\alpha} \right) \frac{e^{-(n\pi/\alpha)(x_s - x_3 - t)}}{\varphi_r(n\pi i/\alpha) + i\chi_r(n\pi i/\alpha)}. \quad (4.7)$$

Using the asymptotic expansions of the Bessel functions for large arguments, it is

possible to show that

$$\mathcal{R}(t) = 8 h_w^{-1/4} H \sum_{n=1}^{+\infty} (-1)^{n+1} n \mathcal{S}^n, \quad (4.8)$$

where

$$\mathcal{S} = \exp \left(-\frac{\pi}{\alpha} (x_s - x_3 - t + 2) \left\{ \frac{h_w^{1/2} - h_1^{1/2}}{m_1} + \frac{h_1^{1/2} - h_2^{1/2}}{m_2} + \frac{h_2^{1/2} - h_3^{1/2}}{m_3} \right\} \right). \quad (4.9)$$

This series is of the form $\sum (-1)^{n+1} n \mathcal{S}^n$ and its maximum is exactly 1/4. Then, the maximum runup R is given by

$$R = 2 h_w^{-1/4} H. \quad (4.10)$$

We note that the maximum runup depends only on the incoming wave height H and on the initial depth at the wall h_w . Interestingly, there is no dependence on any of the slopes, suggesting that this result would only be valid for extremely long waves. Note for example that as $h_w \rightarrow 1$, this result reduces to $R = 2H$, which is the classical solution for the maximum runup on a vertical wall. We will examine the usefulness of (4.10) next.

4.1.2. Comparison between laboratory experiments and analytical predictions

We conducted a series of laboratory experiments with the Revere Beach physical model described earlier. The wavemaker was located 23.22 m away from the wall. Ten capacitance wave gauges were located to record time histories of free surface displacements, as shown in figure 4. Wave gauge number four was always moved to the same relative location from the toe of the composite beach, i.e. at half the wavelength of the solitary wave to be generated ($L/2 = (d/\gamma) \operatorname{arccosh} \sqrt{20}$). This gauge was used to define the height of the solitary wave, and ensured that all waves propagated the same relative distance $L/2$ between the reference location and the toe of the beach; since Synolakis (1987), this is the standard method for referencing the initial wave height for comparisons of the results with theoretical predictions. We conducted experiments at two different water depths, 18.8 cm and 21.8 cm, with eleven and thirteen different H , respectively. With repetitions to check repeatability, a total 31 experiments were run. The difference between the two cases was that for $d = 18.8$ cm there was 1.7 cm depth at the wall; when $d = 21.8$ cm there was 4.7 cm depth at the wall.

In figures 5 and 6 we compare the analytical results of the time histories of the free surface displacements with the laboratory results, at six different locations, for $d = 18.8$ cm and $d = 21.8$ cm. We observed that the linear theory provides satisfactory estimates for the maximum wave height and for the shape of the free surface displacements, especially far from shore and for the longer waves, as expected.

Figure 7 compares the predictions of the asymptotic result (4.10) for the maximum runup with the laboratory data for both depths, as a function of the incident wave height. The solid lines which represent equation (4.10) are drawn to the extent allowed by theory, i.e. until the waves break. The agreement is reasonable at least with all the $d = 18.8$ cm data; the agreement is equally good with the $d = 21.8$ cm data, except for waves smaller than $H = 0.001$. One reason is that these waves are very long and there is not enough propagation distance in the physical model from generation to the toe of the composite beach for the initial solitary wave profile to fully develop. Notice the drastic increase in the maximum runup height at the larger depth; as the

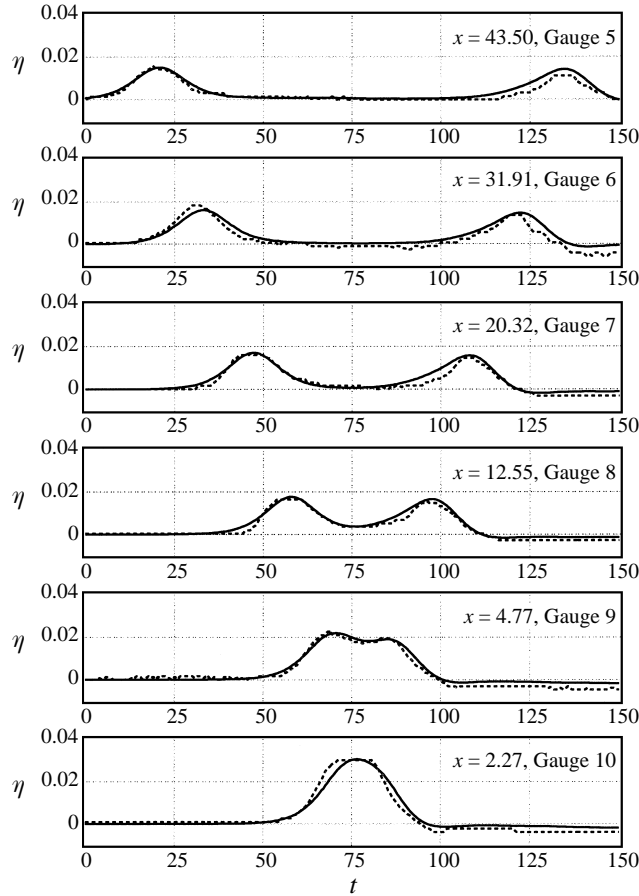


FIGURE 5. Comparison of the time histories of surface elevation between the analytical solution and the laboratory data for a $H = 0.015$ solitary wave at six different locations for $d = 18.8$ cm. The dotted line represents the laboratory data.

depth increases the break point moves closer to the wall, until it occurs right on the wall. We conjecture that this dramatic enhancement of the runup is due to the collapse of the trapped air bubble under the plunging wave as it breaks on the wall, as suggested first by Topliss, Cooker & Peregrine (1992).

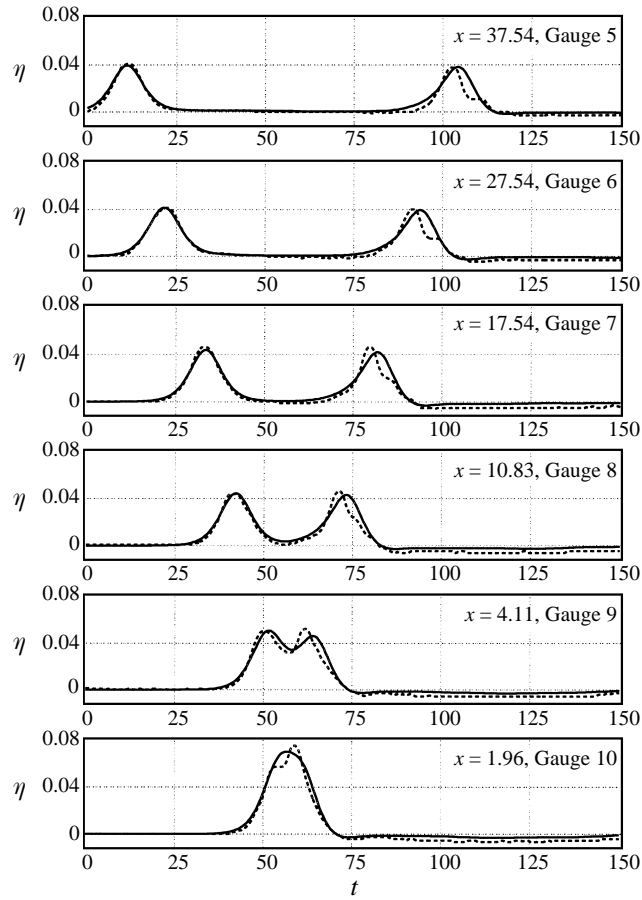
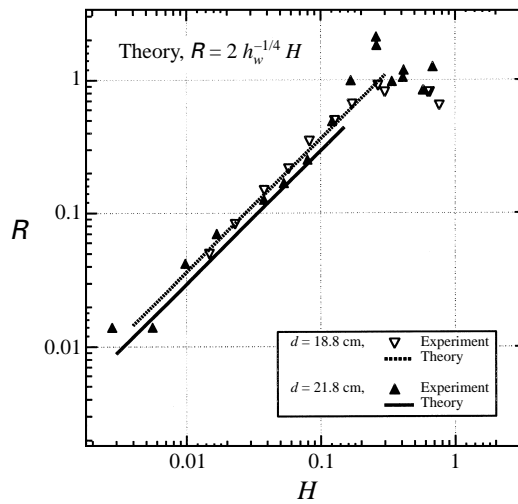
4.2. Two-dimensional topography, the conical island

The overall good agreement between the analytic results and the laboratory data for the Revere Beach suggests the implementation of a similar methodology, i.e. use of piecewise linear topographies for two-dimensional topography. In this section, an extension of the general method presented for one-dimensional topography will be generalized for two-dimensional topography and applied to calculate wave evolution on a conical island.

4.2.1. Analytical solution

We now use the dimensionless two-plus-one linearized equations of motion in two spatial dimensions (x, y) for $\eta(x, y, t)$, i.e.

$$\eta_{tt} = h_0 \nabla^2 \eta + \nabla h_0 \cdot \nabla \eta, \quad (4.11)$$

FIGURE 6. As figure 5 but $H = 0.039$ and $d = 21.8$ cm.FIGURE 7. Comparison of the maximum runup between the analytical solution and the laboratory data for two different depths $d = 18.8$ cm and $d = 21.8$ cm.

where x increases seaward and $\nabla^2 \equiv \partial^2/\partial x^2 + \partial^2/\partial y^2$ and $h_0(x, y)$ is the undisturbed water depth. When the topography has rotational invariance, i.e. $h_0(x, y) = h_0(r, \theta) = h_0(r)$, then $\eta(r, \theta, t) = \mathcal{D}(r, \theta) e^{-i\omega t}$. Then, the field equations reduce to one, as follows:

$$\left(\nabla^2 + \frac{\omega^2}{h_0}\right) \mathcal{D} + \frac{1}{h_0} \nabla h_0 \cdot \nabla \mathcal{D} = 0, \quad (4.12)$$

where $\nabla^2 \equiv \partial^2/\partial r^2 + (1/r)(\partial/\partial r) + (1/r^2)(\partial^2/\partial \theta^2)$. Let $\eta \sim e^{in\theta}$ for integer n , so that $\eta(r, \theta, t) = \sum_{n=-\infty}^{+\infty} R(r) e^{i(n\theta - \omega t)}$. Then $R(r)$ satisfies the following differential equation:

$$R'' + \left(\frac{1}{r} + \frac{h'_0}{h_0}\right) R' + \left(\frac{\omega^2}{h_0} - \frac{n^2}{r^2}\right) R = 0. \quad (4.13)$$

Here, prime denotes differentiation with respect to r and ω denotes the frequency.

For a conical island with topography, $h_0 = \alpha(r-a)$, the field equation (4.13) does not have any eigenfunctions in terms of the known functions, because of the singularity at $r = a$. However, for constant depth $h_0(r) = h_c$ the field equation (4.13) takes the form

$$R'' + \frac{1}{r} R' + \left(\frac{\omega^2}{h_c} - \frac{n^2}{r^2}\right) R = 0, \quad (4.14)$$

an equation with eigenfunctions in terms of Bessel functions. The solution is given by

$$\eta(r, \theta, t) = \sum_{n=-\infty}^{+\infty} \{A_n J_n(kr) + B_n Y_n(kr)\} e^{i(n\theta - \omega t)}, \quad (4.15)$$

where $k = \omega/h_c^{1/2}$.

Let the incident wave $\eta_i(r, \theta, t) = A_{n,i} e^{-i(kx + \omega t)}$ approach from infinity for $r \geq b$. Using the identity

$$e^{z(t-1/t)/2} = \sum_{n=-\infty}^{+\infty} t^n J_n(z), \quad (4.16)$$

Abramowitz & Stegun (1964), and substituting $t = -i e^{i\theta}$, it can be shown that

$$e^{-ikx} = \sum_{n=-\infty}^{+\infty} J_n(kr) e^{in(\theta - \pi/2)}, \quad (4.17)$$

and hence the incoming wave can be expanded in a Fourier–Bessel series. Again for the segment $r \geq b$, there are radiated waves which propagate away to infinity. Therefore, outside of the toe of the conical island, the solution is given by

$$\eta(r, \theta, t) = \eta_i + \eta_s = \sum_{n=-\infty}^{+\infty} \{A_{n,i} e^{-in\pi/2} J_n(kr) + A_{n,r} H_n^{(1)}(kr)\} e^{i(n\theta - \omega t)}. \quad (4.18)$$

Given the singularity of the equation of motion for constant slope, one method of removing it is to approximate the conical surface with cylindrical boxes, henceforth

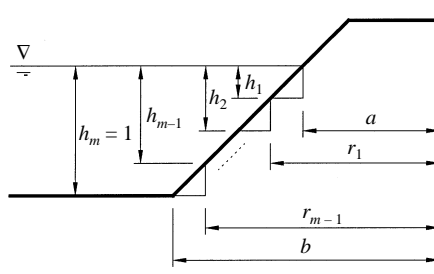


FIGURE 8. Island slope in a stepwise fashion.

referred to as a sills, in a stepwise fashion as in figure 8. Given that the solution is known for evolution over each sill, solving the entire problem involves matching solutions at the interface of the sills. The basic solutions are

$$\eta_j(r, \theta, t) = \sum_{n=-\infty}^{+\infty} e^{i(n\theta - \omega t)} \begin{cases} A_{n,i} e^{-in\pi/2} J_n(kr) + A_{n,r} H_n^{(1)}(kr), & r \geq b, \\ A_n^{(j)} J_n(k_j r) + B_n^{(j)} Y_n(k_j r), & r_{j-1} \leq r \leq r_j, \end{cases} \quad (4.19)$$

where $j = 1, m$ shows the segment number. At the edge of each sill, in other words at a discontinuity in h , η must be continuous so that

$$\eta_j|_{r=r_j} = \eta_{j+1}|_{r=r_j}. \quad (4.20)$$

Moreover, the normal component of the mass flux $h\mathbf{u} \cdot \mathbf{n}$ must also be continuous. Here \mathbf{n} is the unit normal to the discontinuity. Although the vertical acceleration may not be small locally at the discontinuity, it is shown by Bartholomeuz (1958) that this assumption gives correct results for the reflection coefficient of long waves normally incident on a step. In terms of η , this matching condition requires that

$$h_j \frac{\partial \eta_j}{\partial r} \Big|_{r=r_j} = h_{j+1} \frac{\partial \eta_{j+1}}{\partial r} \Big|_{r=r_j}. \quad (4.21)$$

At $r_0 = a$, the following condition must also hold for η :

$$\frac{\partial \eta_1}{\partial r} \Big|_{r=a} = 0. \quad (4.22)$$

For brevity, let us define

$$\kappa_j = k_j r_j = \frac{\omega}{h_j^{1/2}} r_j, \quad \epsilon_j = \frac{k_{j+1}}{k_j} = \left(\frac{h_j}{h_{j+1}} \right)^{1/2}. \quad (4.23)$$

The boundary conditions at the shoreline and each subsequent connection point provide the system of $(2m - 1)$ equations. Instead of solving the system of equations numerically, we will use (2×2) matrices to obtain solutions as described §3, i.e. we obtain the hierarchy of equations

$$\begin{pmatrix} 1 \\ -J'_n(\epsilon_0 \kappa_0) / Y'_n(\epsilon_0 \kappa_0) \end{pmatrix} A_n^{(1)} = \begin{pmatrix} A_n^{(1)} \\ B_n^{(1)} \end{pmatrix}, \quad (4.24)$$

$$\begin{pmatrix} J_n(\kappa_1) & Y_n(\kappa_1) \\ \epsilon_1 J'_n(\kappa_1) & \epsilon_1 Y'_n(\kappa_1) \end{pmatrix} \begin{pmatrix} A_n^{(1)} \\ B_n^{(1)} \end{pmatrix} = \begin{pmatrix} J_n(\epsilon_1 \kappa_1) & Y_n(\epsilon_1 \kappa_1) \\ J'_n(\epsilon_1 \kappa_1) & Y'_n(\epsilon_1 \kappa_1) \end{pmatrix} \begin{pmatrix} A_n^{(2)} \\ B_n^{(2)} \end{pmatrix}, \quad (4.25)$$

$$\begin{pmatrix} J_n(\kappa_2) & Y_n(\kappa_2) \\ \epsilon_2 J_n'(\kappa_2) & \epsilon_2 Y_n'(\kappa_2) \end{pmatrix} \begin{pmatrix} A_n^{(2)} \\ B_n^{(2)} \end{pmatrix} = \begin{pmatrix} J_n(\epsilon_2 \kappa_2) & Y_n(\epsilon_2 \kappa_2) \\ J_n'(\epsilon_2 \kappa_2) & Y_n'(\epsilon_2 \kappa_2) \end{pmatrix} \begin{pmatrix} A_n^{(3)} \\ B_n^{(3)} \end{pmatrix}, \quad (4.26)$$

$$\begin{aligned} & \vdots \\ \begin{pmatrix} J_n(\kappa_{m-1}) & Y_n(\kappa_{m-1}) \\ \epsilon_{m-1} J_n'(\kappa_{m-1}) & \epsilon_{m-1} Y_n'(\kappa_{m-1}) \end{pmatrix} & \begin{pmatrix} A_n^{(m-1)} \\ B_n^{(m-1)} \end{pmatrix} \\ & = \begin{pmatrix} e^{-in\pi/2} J_n(\epsilon_{m-1} \kappa_{m-1}) & H_n^{(1)}(\epsilon_{m-1} \kappa_{m-1}) \\ e^{-in\pi/2} J_n'(\epsilon_{m-1} \kappa_{m-1}) & H_n^{(1)' }(\epsilon_{m-1} \kappa_{m-1}) \end{pmatrix} \begin{pmatrix} A_{n,i} \\ A_{n,r} \end{pmatrix}. \end{aligned} \quad (4.27)$$

Here again, a prime represents differentiation with respect to the argument. These equations can be rewritten as

$$S_1 A_n^{(1)} = V_1, \quad (4.28)$$

$$S_{11} V_1 = S_{12} V_2, \quad (4.29)$$

$$S_{22} V_2 = S_{23} V_3, \quad (4.30)$$

$$\vdots$$

$$S_{m-1m-1} V_{m-1} = S_{m-1m} V_m. \quad (4.31)$$

On combining, we obtain,

$$S_{m-1m}^{-1} S_{m-1m-1} \cdots S_{33} S_{23}^{-1} S_{22} S_{12}^{-1} S_{11} S_1 A_n^{(1)} = V_m. \quad (4.32)$$

We specify the boundary condition as before; for an incident wave of the form $\eta(x, t) = \int_{-\infty}^{+\infty} \Phi(\omega) e^{-i\omega t} d\omega$, then the transmitted wave in each segment is given by

$$\eta_j(r, \theta, t) = \int_{-\infty}^{+\infty} \Phi(\omega) \sum_{n=-\infty}^{+\infty} \{A_n^{(j)} J_n(k_j r) + B_n^{(j)} Y_n(k_j r)\} e^{i(n\theta - \omega t)} d\omega, \quad (4.33)$$

where j shows the segment number and $\Phi(\omega)$ is the Fourier transform of the initial solitary wave profile as in Synolakis (1986). To determine the maximum runup, the integral (4.33) can be written in the form

$$\eta_1(a, \theta, t) = \int_{-\infty}^{+\infty} \Phi(\omega) \sum_{n=-\infty}^{+\infty} \{A_n^{(1)} J_n(k_1 a) + B_n^{(1)} Y_n(k_1 a)\} e^{i(n\theta - \omega t)} d\omega, \quad (4.34)$$

for the first segment. Note that $B_n^{(1)}$ can be found in terms of $A_n^{(1)}$ from equation (4.28) while $A_n^{(1)}$ can be determined in terms of $A_{n,i}$ using the matrix equation (4.32). Equation (4.34) then takes the form

$$R(t) = \eta_1(a, \theta, t) = (2/3) \int_{-\infty}^{+\infty} \omega \operatorname{cosech}(\alpha\omega) \sum_{n=-\infty}^{+\infty} \frac{e^{i\theta}}{\varphi + i\chi} d\omega, \quad (4.35)$$

where

$$\varphi = J_n'(\epsilon_{m-1} \kappa_{m-1}) C(1) - J_n(\epsilon_{m-1} \kappa_{m-1}) C(2), \quad (4.36)$$

$$\chi = Y_n'(\epsilon_{m-1} \kappa_{m-1}) C(1) - Y_n(\epsilon_{m-1} \kappa_{m-1}) C(2), \quad (4.37)$$

$$C = S_{m-1m-1} \cdots S_{33} S_{23}^{-1} S_{22} S_{12}^{-1} S_{11} S_1 / (\Delta_0 \Delta_{m-1}), \quad (4.38)$$

$$\Delta_0 = J_n(\epsilon_0 \kappa_0) - J_n'(\epsilon_0 \kappa_0) Y_n(\epsilon_0 \kappa_0) / Y_n'(\epsilon_0 \kappa_0), \quad (4.39)$$

$$\Delta_{m-1} = J_n(\epsilon_{m-1} \kappa_{m-1}) Y_n'(\epsilon_{m-1} \kappa_{m-1}) - J_n'(\epsilon_{m-1} \kappa_{m-1}) Y_n(\epsilon_{m-1} \kappa_{m-1}), \quad (4.40)$$

$$\Theta = n\theta + \omega(x_s - t) + (-n + 1)\pi/2. \quad (4.41)$$

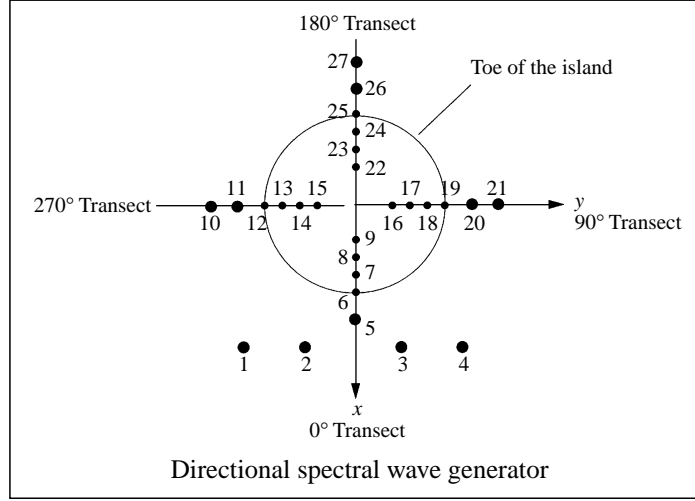


FIGURE 9. A sketch of the basin for the conical island. The numbers refer to the wave gauges. This drawing is not to scale.

We use asymptotic expansions for the large arguments of the Bessel functions, and we note that the contribution from each $S_{jj}S_{j-1j}^{-1}$ term in the matrix equation (4.32) is $(r_{j-1}/r_j)^{1/2}\mathbf{I}$, where \mathbf{I} is the unit matrix; this allows us to write $(a/b)^{1/2}S_{m-1m}^{-1}S_{11}V_1 = V_m$. Therefore, the solution for the free surface displacement at the shoreline is given by

$$R(t) = \frac{(4/3)}{\pi(ab)^{1/2}} \int_{-\infty}^{+\infty} \operatorname{cosech}(\alpha\omega) \sum_{n=-\infty}^{+\infty} \frac{e^{i\theta}}{H_n^{(1)'}(\omega b)} d\omega. \quad (4.42)$$

This equation resembles the exact solution for wave runup on a cylinder of radius a (Isaacson 1983), which is given by

$$R(t) = \frac{(4/3)}{\pi a} \int_{-\infty}^{+\infty} \operatorname{cosech}(\alpha\omega) \sum_{n=-\infty}^{+\infty} \frac{e^{i\theta}}{H_n^{(1)'}(\omega a)} d\omega. \quad (4.43)$$

It can be seen from the last two equations that as $b \rightarrow a$, i.e. as the conical island turns into a circular cylinder, equation (4.42) turns into equation (4.43), one preliminary check of the accuracy of the asymptotic manipulation. One interesting feature of equation (4.42) is the explicit dependence of the runup on the square root of the diameter of the initial shoreline a , suggesting that for fixed b , the runup decreases as a increases. Since the slope of the conical surface of the island $1/(b-a)$ increases, as a increases, the runup decreases with the slope. This is compatible with the findings of Liu *et al.* (1995), who calculated numerically the relative runup of an $H = 0.1$ wave with initial solitary wave profiles as $R/H = 2.92$, 2.73 and $R/H = 2.34$ up three different beach slopes $\cot \beta = 4$, 2.75 and $\cot \beta = 1.73$ respectively. Reluctant as we are to draw conclusions from only three data points, it is quite intriguing that a simple calculation shows that Liu *et al.*'s (1995) numerical results suggest that the runup varies as $a^{-1/2}$, just as (4.42) implies.

4.2.2. Experimental method

We performed laboratory experiments at Coastal Engineering Research Center in a basin 30 m wide and 25 m long. A sketch of the basin is shown in figure 9. These

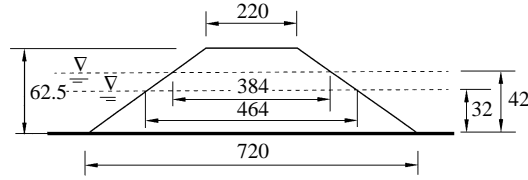
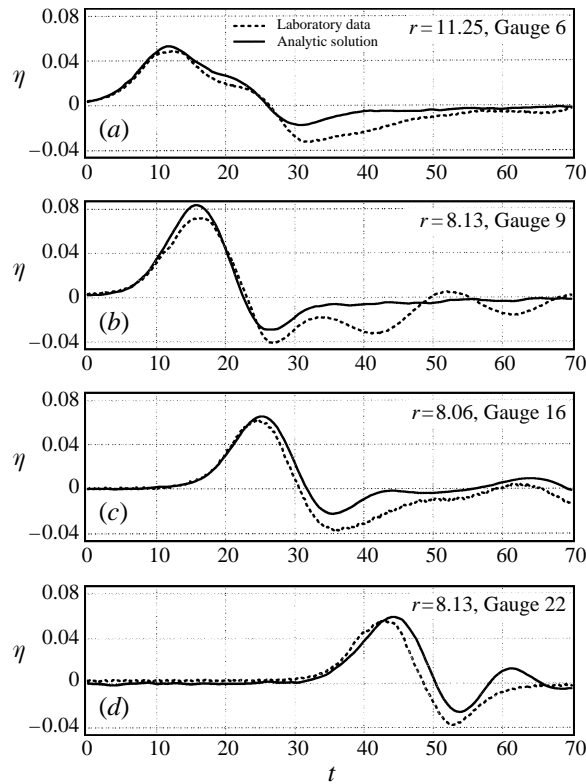


FIGURE 10. Conical island topography. All dimensions are in cm. This drawing is not to scale.


 FIGURE 11. Comparison of the time histories of surface elevation between the analytical solution and the laboratory data for a $H = 0.045$ solitary wave at different gauges for $d = 32$ cm.

experiments are described elsewhere in greater detail (Liu *et al.* 1995; Briggs *et al.* 1994; Kânoğlu 1996). Briefly, we used a directional spectral wave generator (DSWG) which is located at $x = 12.96$ m to generate waves with an initial solitary wave-like profile. The 27.432 m long DSWG consists of sixty 46 cm wide and 76 cm high individual paddles, each of which can be driven independently.

In the physical model, a 60 cm high, 7.2 m toe diameter and 2.2 m crest diameter circular island with a 1:4 slope shown in figure 10 was located in the basin. Experiments were conducted at two different water depths, with dimensionless solitary wave heights H equal to 0.045, 0.091 and 0.181 at 32 cm depth and with H equal to 0.046, 0.073 and 0.091 at 42 cm depth. We repeated each experiment at least twice, and we measured the maximum runup heights around the perimeter of the island at twenty four locations.

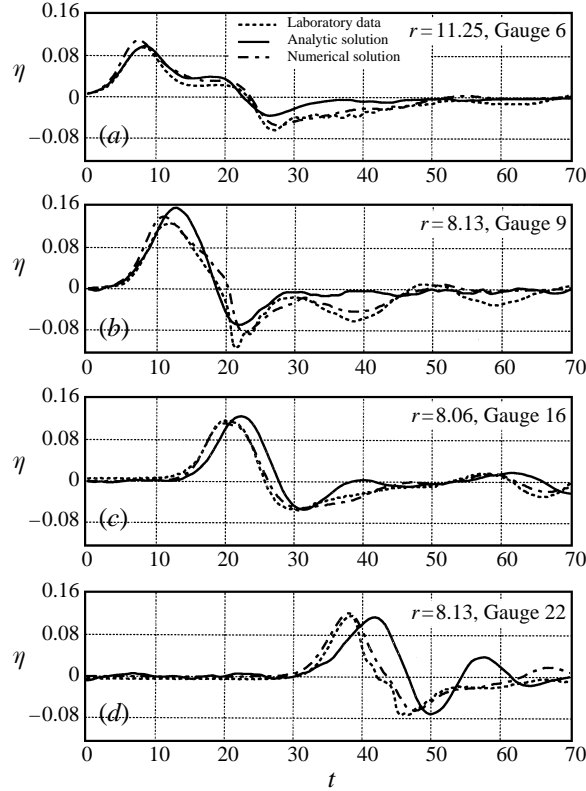
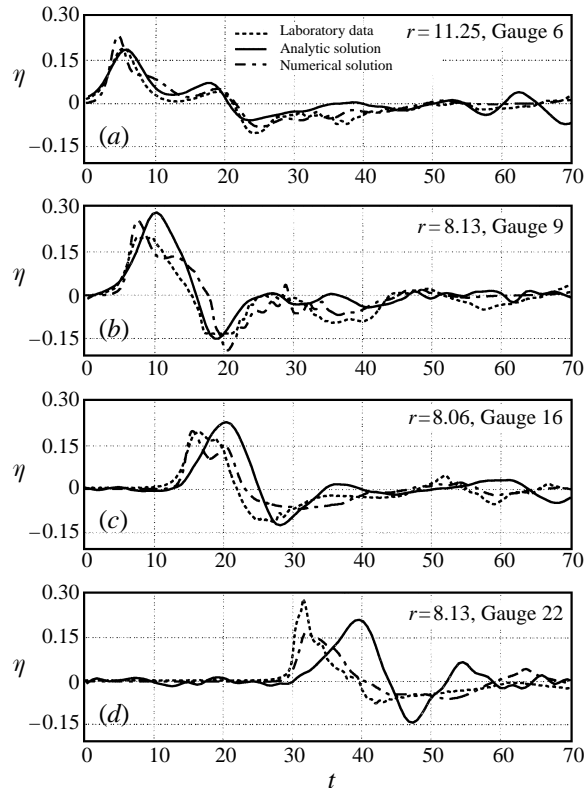


FIGURE 12. Comparison of the time histories of surface elevation among the linear theory predictions, the numerical nonlinear theory results and the laboratory data for a $H = 0.091$ solitary wave at different gauges for $d = 32$ cm.

4.2.3. Comparisons between laboratory experiments and analytical results

We evaluate the integral (4.33) with IMSL routines to determine the time histories of the surface elevations for the analytical solution at different gauge locations. Comparisons between the linear theory predictions, and the laboratory data for the time histories of the surface elevations are shown in figure 11 for the $H = 0.045$ wave at 32 cm depth; linear theory predicts the wave evolution adequately, although on the back side of the island (figure 11d), the agreement is poor. Comparisons among the linear theory predictions, numerical nonlinear theory results and the laboratory data are shown in figures 12 and 13 for an $H = 0.091$ and $H = 0.181$ wave at 32 cm depth; the nonlinear theory predictions are from Titov & Synolakis (1997a). The agreement between the linear theory and the nonlinear theory predictions is only good at the toe of the island; as the wave evolves, the nonlinear theory predicts the evolution well on the front, but not at the sides and on the back, a reflection of the fact that the wave breaks, and the breaking propagates along the wavefront. A second-order factor which may account for a small part of the differences between linear and nonlinear results is that in the nonlinear theory predictions the numerical model used the actual wavemaker trajectory and it calculated the wave evolution from the DSWG to the island; in our linear theory analysis, we only assume a solitary wave profile with crest height as determined from the


 FIGURE 13. As figure 12 but for a $H = 0.181$ solitary wave.

laboratory to predict the evolution. As it has been pointed by Briggs *et al.* (1994), only the front surface of the solitary-wave profiles produced by the DSWG fit the Boussinesq profile accurately; the back side of the waves fit the profile less well, and there was a tail. Also, note that both of these waves ($H = 0.091$ and 0.181) are quite large and not in the range of geophysical interest; had it been possible to generate waves in the range 0.001 to 0.0001 in our basin, the agreement between the linear theory results and the physical experiments might have been much better.

Comparisons between the laboratory experiments and the analytical solution for the maximum runup heights are shown in figures 14–15. We calculate the integral (4.34) with IMSL routines to determine the maximum runup heights for the analytical theory. Figure 14 shows the maximum runup variation around the island as a function of the angle θ , with $\theta = 0$ directly on the front of the island and with θ increasing counterclockwise, for three different wave heights, $H = 0.045$, 0.091 and 0.181 at the 32 cm depth. The agreement is uniformly good at the front of the island, but poor by comparison at the sides and at the lee side. Note that in the laboratory experiments, wave breaking was observed on the lee side of the island for the $H = 0.091$ and $H = 0.181$ waves; the enhanced runup is due to the strong interaction of the two trapped waves, as shown in the photographs, figures 16 and 17.

Similar conclusions can be drawn from figure 15 which shows the maximum runup variation for $H = 0.046$, 0.073 and 0.091 waves at the 42 cm depth. Notice that even though the $H = 0.045$ wave at 32 cm depth has the same maximum runup on the

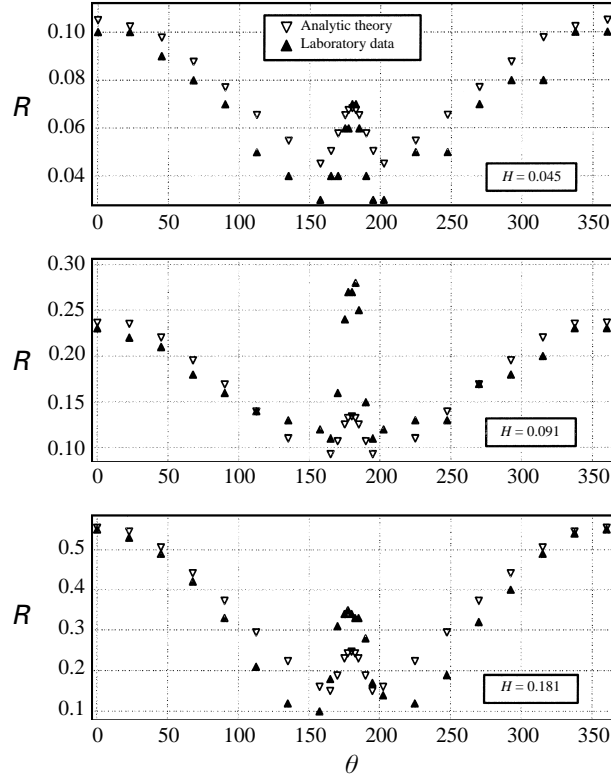


FIGURE 14. Comparison of the maximum runup heights between the analytical solution and the laboratory data for three different incident wave heights H at $d = 32$ cm.

front of the island as the $H = 0.046$ wave at the 42 cm depth, there is enhanced runup of the $H = 0.046$ wave at 42 cm on the lee side, not observed with the runup of the $H = 0.045$ wave in the 32 cm depth experiments. This underscores the effect of the wet diameter of the shoreline in the wave energy trapping, as discussed earlier: when $d=32$ cm, the diameter of the wet perimeter of the island is $2a = 14.5$, while when $d=42$ cm, $2a = 9.14$.

In general, the differences between the linear theory predictions and the laboratory results increase as H increases, as expected. Nonlinear effects are more important for the larger waves; what is unexpected is that the result derived from the linear theory solution produces credible predictions on the front side of the island, even for the $H = 0.181$ wave at 32 cm. Clearly, calculations using a higher-order theory are needed to predict accurately the runup around the island.

Finally, we investigated the effects of the number of steps in our solutions. In numerical solutions of the NSW, the spacial grid length affects the runup predictions; N. Shuto (private communication) suggested that dividing the conical surface into stepwise topography might have a similar effect. Therefore, we considered 5, 10 and 15 steps over the sloping region of the conical island and we present the results in figure 18. The effect of the number of steps on the runup predictions is about 10%, in the same order as the effect of grid resolution in state-of-the-art numerical inundation computations over plane beaches.

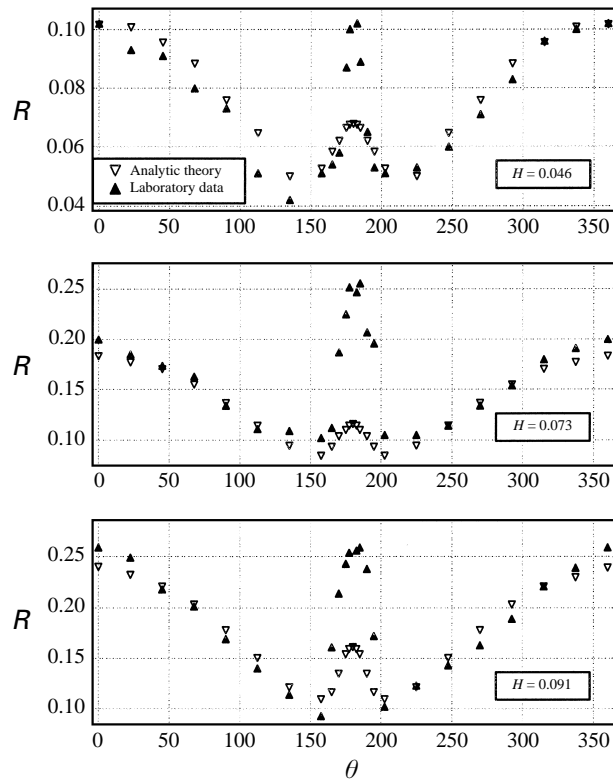


FIGURE 15. As figure 14 but at $d = 42$ cm.

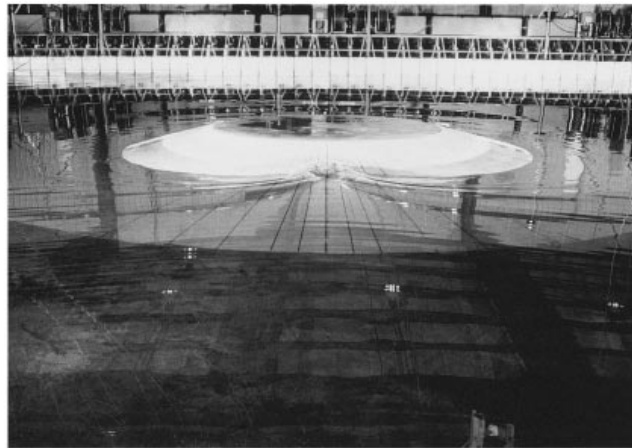


FIGURE 16. A view of the conical island and the directional spectral wave generator from the back side of the island.

5. Conclusions

We have presented an analytical method for determining the wave evolution for one-dimensional piecewise linear topographies and we have extended this method to the two-dimensional topography of a conical island. Our method allows the explicit determination of the wave evolution and runup in terms of special functions by

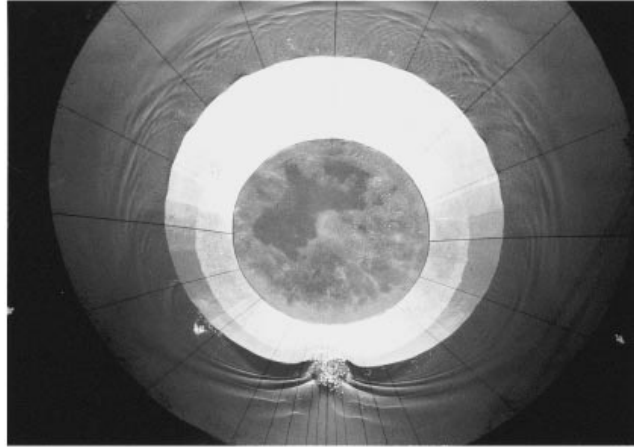


FIGURE 17. An overhead photograph showing wave runup on the lee side of the island.

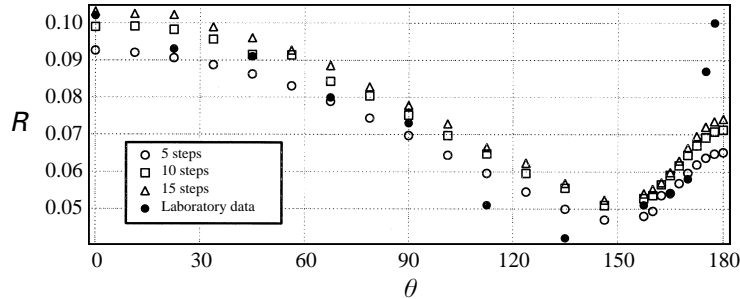


FIGURE 18. Comparison of the maximum runup heights for different numbers of steps, i.e. 5, 10 and 15 steps; $H = 0.046$, $d = 42$ cm.

multiplication of simple rank-2 matrices, and it makes simple asymptotic analysis possible to identify important physical parameters.

We applied our method using waves which offshore had the profile of a solitary wave to the topographies of a composite beach slope with two linear segments. We found that contrary to what one would have expected if one argued that long waves interact with topography as they do with a vertical wall, the runup of solitary waves depends only on the slope closest to the shoreline for a large range of transition depths; we confirmed our result using numerical solutions of the NSW. For the Revere Beach consisting of three linear segments and a vertical wall, we found that the runup is primarily determined by the depth at the wall, and we have verified our asymptotic result through comparisons with laboratory data. Finally we found that the runup of long waves on a conical island is inversely proportional to the square root of the product of the initial shoreline diameter and the diameter at the toe of the island, thereby confirming earlier numerical and laboratory results which had suggested that wave trapping depends on the initial shoreline diameter and on the island slope but had not been able to identify the correct scaling.

We conclude that the runup of long waves on piecewise linear topographies is not as straightforward as often assumed, suggesting that the practice of inferring the maximum runup from the numerical computations which stop the evolution at an arbitrary threshold depth and use that value to infer the runup may be inappropriate

for certain waves; detailed runup or inundation computations are almost invariably necessary for accurate predictions.

We are grateful to Dr Cliff Astill of the National Science Foundation for supporting our work through grants (BCS-9201326 and CMS-9614221), and to Professor Nobuo Shuto for certain interesting suggestions. We would also like to thank also Mike Briggs, Gordi Harkins and Deborah Green of the Coastal Engineering Research Center and Alan Collinge of University of Southern California for their contributions during the experimental phase of this study.

REFERENCES

- ABE, K. & ISHIL, H. 1980 Propagation of tsunami on linear slope between two flat regions, Part 2 – reflection and transmission. *J. Phys. Earth* **28**, 543–552.
- ABRAMOWITZ, M. & STEGUN, I. A. 1964 *Handbook of Mathematical Functions*. Dover.
- BARTHOLOMEUZ, E. F. 1958 The reflection of long waves at a step. *Proc. Camb. Phil. Soc.* **54**, 106–118.
- BRIGGS, M. J., SYNOLAKIS, C. E., HARKINS, G. S. & GREEN, D. 1994 Laboratory experiments of tsunami runup on a circular island. *PAGEOPH* **144** (3/4), 569–593.
- BROCCHINI, M. & PEREGRINE, D. H. 1996 Integral flow properties of swash zone and averaging. *J. Fluid Mech.* **317**, 241–273.
- CARRIER, G. F. 1966 Gravity waves on water of variable depth. *J. Fluid Mech.* **24**, 641–659.
- CARRIER, G. F. 1993 Tsunami propagation from a finite source. *Proc. IUGG/IOC Intl Tsunami Symp. Wakayama, Japan*, pp. 410–427. Japan. Society of Civil Engineers.
- CARRIER, G. F. & NOISEUX, C. F. 1983 The reflection of obliquely incident tsunamis. *J. Fluid Mech.* **133**, 147–160.
- DEVILLARD, P., DUNLOP, F. & SOUILLARD, B. 1988 Localization of gravity waves on a channel with a random bottom. *J. Fluid Mech.* **186**, 521–538.
- EVANS, D. V. & LINTON, C. M. 1994 On step approximations for water–wave problems. *J. Fluid Mech.* **278**, 229–249.
- GERRARD, A. & BURCH, J. M. 1987 *Introduction to Matrix Methods in Optics*. University Microfilms International (John Wiley & Sons).
- GORING, D. G. 1978 Tsunamis—the propagation of long waves onto a shelf. *W. M. Keck Laboratory of Hydraulics and Water Resources, Division of Engineering and Applied Science, California Institute of Technology. Rep.* KH-R-38.
- GRILLI, S. 1996 Boundary integral equation methods used for long wave runup prediction models. *Long Wave Runup Models* (ed. H. H. Yeh *et al.*) pp. 116–180. World Scientific.
- HAMILTON, J. 1977 Differential equations for long–period gravity waves on fluid of rapidly varying depth. *J. Fluid Mech.* **83**, 289–310.
- HOMMA, S. 1950 On behaviour of seismic sea waves around the circular island. *Geophys. Mag.* **21**, 199–208.
- ISAACSON, M. Q. 1983 Solitary wave diffraction around large cylinder. *J. Waterway, Port, Coastal Ocean Engng* **109**, 121–127.
- KÂNOĞLU, U. 1996 The runup of long waves around piecewise linear bathymetries. PhD Thesis. University of Southern California, Los Angeles.
- KELLER, J. B. & KELLER, H. B. 1964 Water wave run–up on a beach. *ONR Research Rep.* Contract NONR-3328(00). Dept. of the Navy, Washington, DC. 40 pp.
- KOBAYASHI, N. & KARJADI, E. A. 1994 Surf–similarity parameter for breaking solitary–wave runup. *J. Waterway, Port, Coastal Ocean Engng* ASCE **120**, 56–73.
- LAUTENBACHER, C. C. 1970 Gravity wave refraction by island. *J. Fluid Mech.* **41**, 655–672.
- LIU, P. L.-F., CHO, Y.-S., BRIGGS, M. J., KANOGLU, U. & SYNOLAKIS, C. E. 1995 Runup of solitary waves on a circular island. *J. Fluid Mech.* **320**, 259–285.
- LIU, P. L.-F., SYNOLAKIS, C. E. & YEH, H. 1991 Report on the international workshop on long–wave run–up. *J. Fluid Mech.* **229**, 675–688.
- LONGUET-HIGGINS, M. S. 1967 On trapping of wave energy round islands. *J. Fluid Mech.* **29**, 781–821.
- MILES, J. W. 1967 Surface–wave scattering matrix for a shelf. *J. Fluid Mech.* **28**, 755–767.

- NACHBIN, A. & PAPANICOLAOU, G. C. 1992 Water waves in shallow channels of rapidly varying depth. *J. Fluid Mech.* **241**, 311–332.
- NEU, W. L. & SHAW, R. P. 1981 Long wave scattering by linear segmented bottom topographies. *Rep. 123*. Dept. of Engng Sci., SUNY at Buffalo, Buffalo, NY.
- NEU, W. L. & SHAW, R. P. 1987 Tsunami filtering by ocean topography. *Ocean Phys. and Engng* **12**, 1–23.
- PROVIS, D. G. 1975 Propagation of water waves near an island. PhD Thesis, University of Essex.
- SATAKE, K., BOURGEOIS, J., ABE, K., ABE, K., TSUJI, Y., IMAMURA, F., IO, Y., KATAO, H., NOGUERA, E. & ESTRADA, F. 1993 Tsunami field survey of the 1992 Nicaragua earthquake. *EOS Trans. AGU* **74**(13), 145–156.
- SHAW, R. P. 1974 Long waves on linear topographies. *JTRE Internal Rep.* 119. Joint Tsunami Research Effort, University of Hawaii, Honolulu, Hawaii.
- SHAW, R. P. & NEU, W. L. 1988 Long wave trapping by axisymmetric topographies. In *Natural and Man-made Hazards* (ed. M. I. El-Sabh & T. S. Murty), pp. 227–238.
- SHEN, M. C., MEYER, R. E. & KELLER, J. B. 1968 Spectra of water waves in channels and around island. *Phys. Fluids* **11**, 2289–2304.
- SHUTO, N. 1991 Numerical simulation of tsunamis. In *Tsunami Hazard* (ed. E. Bernard), pp. 171–191. Kluwer.
- SMITH, R. & SPRINKS, T. 1975 Scattering of surface waves by a conical island. *J. Fluid Mech.* **72**, 373–384.
- SPRINKS, T. & SMITH, R. 1983 Scale effects in a wave refraction experiment. *J. Fluid Mech.* **129**, 455–471.
- SYNOLAKIS, C. E. 1986 The runup of long waves. PhD Thesis, California Institute of Technology, Pasadena.
- SYNOLAKIS, C. E. 1987 The runup of solitary waves. *J. Fluid Mech.* **185**, 523–545.
- SYNOLAKIS, C. E., LIU, P. L.-F., CARRIER, G. & YEH, H. 1997 Tsunamigenic Sea-floor Deformations. *Science* **278**, 598–599.
- SYNOLAKIS, C. E., IMAMURA, F., TSUJI, Y., MATSUTOMI, S., TINTI, B., COOK, B. & USHMAN, M. 1995 Damage, Conditions of east Java tsunami of 1994 analyzed. *EOS Trans. AGU* **76**(26), 257 and 261–262.
- TAKAHASHI, TO., TAKAHASHI, TA., SHUTO, N., IMAMURA, F. & ORTIZ, M. 1995 Source models for the 1993 Hokkaido–Nansei–Oki earthquake tsunami. *Pure Appl. Geophys.* **144**, 747–768.
- TINTI, S. & VANNINI, C. 1994 Theoretical investigation on tsunamis induced by seismic faults near ocean islands. *Marine Geodesy*. **17**, 193–212.
- TITOV, V. V. 1997 Numerical modeling of long wave runup. PhD Thesis, University of Southern California, Los Angeles.
- TITOV, V. V. & SYNOLAKIS, C. E. 1995 Modeling of breaking and nonbreaking long wave evolution and runup using VTCS–2. *J. Harbors, Waterways, Port, Coastal Ocean Engng* **121**, 308–316.
- TITOV, V. V. & SYNOLAKIS, C. E. 1997a Numerical modeling of 2-D and 3-D long wave runup using VTCS–2 and VTCS–3. In *Long Wave Runup Models* (ed. H. H. Yeh *et al.*), pp. 242–248. World Scientific.
- TITOV, V. V. & SYNOLAKIS, C. E. 1997b Extreme inundation flows during the Hokkaido–Nansei–Oki tsunami. *Geophys. Res. Lett.* **24**, 1315–1318.
- TOPLISS M. E., COOKER, M. J. & PEREGRINE, D. H. 1992 Pressure oscillations during wave impact on vertical walls. *Proc. Twenty-Third Intl Coastal Engng Conf.* (ed. B. L. Edge), Vol. 2, pp. 1639–1650. ASCE.
- VASTANO, A. C. & REID, R. O. 1967 Tsunami response for island: Verification of a numerical procedure. *J. Mar. Res.* **25**, 129–139.
- WARD, D. 1995 Physical Model study of Revere Beach, Massachusetts. *US Army Corps of Engineers, Waterways Experiment Station Technical Rep.* CERC–95–2, March 1995.
- WATSON G., BARNES, T. C. D. & PEREGRINE, D. H. 1997 Numerical runup modeling of solitary wave propagation and breaking on a beach and runup on a vertical wall. In *Long Wave Runup Models* (ed. H. H. Yeh *et al.*), pp. 291–298. World Scientific.
- YEH, H., IMAMURA, F., SYNOLAKIS, C. E., TSUJI, Y., LIU, P. L.-F. & SHI, S. 1993 The Flores Island tsunamis. *EOS Trans. AGU* **74** (33), 369, 371–373.
- YEH H., LIU, P. L.-F., BRIGGS M. J. & SYNOLAKIS, C. E. 1994 Tsunami Catastrophe in Babi Island. *Nature* **372**, 6503.
- YEH, H., LIU, P. L.-F. & SYNOLAKIS, C. E. (Eds.) 1997 *Long Wave Runup Models*. World Scientific.